



Catalytic ozonation for the degradation of acetylsalicylic acid in aqueous solution by magnetic CeO₂ nanometer catalyst particles

Qizhou Dai, Jiayu Wang, Jie Yu, Jun Chen, Jianmeng Chen*

College of Biological and Environmental Engineering, Zhejiang University of Technology, Hangzhou 310032, China

ARTICLE INFO

Article history:

Received 18 December 2012
Received in revised form 3 May 2013
Accepted 31 May 2013
Available online 10 June 2013

Keywords:

Catalytic ozonation
Rare earth
Fe₃O₄@SiO₂@CeO₂ nanoparticles
Magnetic catalyst
Reaction mechanism

ABSTRACT

A magnetic core/shell CeO₂ nanometer catalyst particle of Fe₃O₄@SiO₂@CeO₂ for ozonation was prepared and the catalytic activity was evaluated by the degradation of acetylsalicylic acid (ASA). The characterizations of the magnetic nanoparticles, such as TEM, XRD and EDX, showed that Fe₃O₄@SiO₂@CeO₂ had a ternary structure with a Fe₃O₄ magnetic core, a silica membrane mid-layer and CeO₂ outer layer. The catalysts of Fe₃O₄@SiO₂@CeO₂ showed an obviously high efficiency in catalytic ozonation on the degradation of ASA, and thus could also enhance the TOC removal. The ASA removal with Fe₃O₄@SiO₂@CeO₂ catalyst at 60 min could reach 81.0%, while 67.3% with Fe₃O₄@SiO₂, 66.1% with Fe₃O₄ and only 64.1% with ozonation alone. Fe₃O₄@SiO₂@CeO₂ catalysts could also enhance the ozone utilization during the reaction. The effect of radical scavengers showed that the high removal efficiency of catalytic ozonation over Fe₃O₄@SiO₂@CeO₂ may be mainly attributed to surface reactions. According to stability and recyclability test of the Fe₃O₄@SiO₂@CeO₂ catalysts, the results showed that the catalysts would be helpful in the separation and magnetic recyclability. In addition, based on the intermediates detected by GC/MS, a possible degradation pathway of ASA was proposed.

© 2013 Elsevier B.V. All rights reserved.

1. Introduction

Ozonation is considered to be a good wastewater treatment technique because of its strong oxidizing, environmentally friendly and its potential applications in field of environmental science, and it has been receiving widespread attention [1–5]. The organic pollutants in wastewater can be removed by direct oxidation in relatively slow and selective fashion or by indirect oxidation in faster and less selective way [6,7]. However, the application of ozonation is still limited due to the oxidation selectivity and relatively low efficiency [8,9]. Therefore, to overcome the limitation of ozonation and enhance the economic efficiency, a lot of improved processes based on the ozonation were developed [10–13]. Recently, catalytic ozonation especially heterogeneous catalytic ozonation has attracted a lot of attention because it can enhance the removal of refractory compounds with relatively high efficiency [7,14].

The catalyst plays an important role in heterogeneous catalytic ozonation [13,15,16]. Transition metal oxides and rare earth oxides, such as MnO₂, TiO₂, Ni₂O₃, Al₂O₃, Co₃O₄, CuO, ZnO, V₂O₅, CeO₂, La₂O₃, and Pr₆O₁₁, are usually chosen as catalysts [13,15,17–22]. Among these, CeO₂ is considered to be a promising catalyst for catalytic ozonation because of its biological and chemical inertness, strong oxidizing power, cyclic usability as well as extended

stability against chemical corrosion [17,23–27]. Faria et al. [23] reported that ceria (Ce–O) and a novel ceria-activated carbon composite (AC₀–Ce–O) were prepared, and Ce–O showed a great catalytic effect, especially in the ozonation of oxalic acid. Thereafter, Li et al. [24] reported that cerium supported on activated carbon (Ce/AC), which was prepared by dipping method, was employed to degrade dimethyl phthalate (DMP) in water and showed the catalytic activity was significant. Subsequently, Martins et al. [25] prepared multivalent Mn–Ce–O by co-precipitation process, and its catalytic ozonation activity was evaluated by the decomposition of six acids, showing the high removal efficiency. Since the CeO₂ catalysts possess good catalytic ozonation ability, it deserves particular attention and should be widely used.

However, the way to effectively immobilize or separate the CeO₂ particles is still a challenge in this catalytic ozonation system. Magnetic separation using magnetically recoverable nanoparticles offers a promising approach to solve this problem [28,29]. Therefore, a type of magnetically separable composite catalyst comprises a CeO₂ shell and a magnetic core, making them recoverable due to their magnetic properties [30]. A lot of materials, such as Fe₃O₄, γ-Fe₂O₃, black sand, NiFe₂O₄, CoFe₂O₄, and FeCo, have the magnetic properties and can be used as the core [28,31–35]. Among them, Fe₃O₄ has been chosen because of its remarkable magnetic properties and low toxicity [29,36,37]. In addition, there is a silica layer between the magnetic core and the CeO₂ shell, and this structure can avoid the oxidation of the Fe₃O₄ core by the outer atmosphere [38–40]. Moreover, silica covered on the surface of magnetic

* Corresponding author. Tel.: +86 571 88320276; fax: +86 571 88320882.
E-mail address: jchen@zjut.edu.cn (J. Chen).

microspheres prevents the aggregation induced by the magnetic dipolar attraction between magnetic nanoparticles, because silica covered on the surface of magnetic microspheres, satisfied results can be reached at a certain condition, and the remaining magnetization become lower, thus enhanced a better dispersion of magnetic nanoparticles in suspension [38,40]. However, few studies on this kind of core/shell catalyst and catalytic ozonation of pharmaceutical wastewater by this kind of catalyst have been reported.

Herein, we prepared unique $\text{Fe}_3\text{O}_4@\text{SiO}_2@\text{CeO}_2$ catalyst with the structure of a Fe_3O_4 magnetic core, a silica membrane mid-layer and CeO_2 outer layer. Acetylsalicylic acid (ASA) was selected as model pollutant to evaluate the catalytic ozonation activity. A possible degradation pathway of ASA and the reaction mechanism of ozonation catalyzed by $\text{Fe}_3\text{O}_4@\text{SiO}_2@\text{CeO}_2$ catalyst were proposed. The characterization techniques used to probe these catalysts were XRD, FT-IR, TEM, SEM, and EDX. In addition, stability and recyclability of the $\text{Fe}_3\text{O}_4@\text{SiO}_2@\text{CeO}_2$ catalysts were also discussed.

2. Materials and methods

2.1. Reagents

ASA was selected as the model pollutant, and was obtained from Shanghai J&K Chemical Reagent (China) Co., Ltd. (purity 99%). Tert-butyl alcohol (TBA) was chosen as the radical scavenger and purchased from Shanghai Lingfeng Chemical Reagent (China) Co., Ltd. The ferrous sulfate heptahydrate ($\text{FeSO}_4 \cdot 7\text{H}_2\text{O}$), potassium hydroxide (KOH), potassium nitrate (KNO_3), trisodium citrate, ammonium hydroxide ($\text{NH}_3 \cdot \text{H}_2\text{O}$), ethyl alcohol ($\text{C}_2\text{H}_5\text{OH}$), tetraethyl orthosilicate (TEOS), cerous nitrate ($\text{Ce}(\text{NO}_3)_3 \cdot 6\text{H}_2\text{O}$), used for the preparation of $\text{Fe}_3\text{O}_4@\text{SiO}_2@\text{CeO}_2$ catalyst were of analytical grade and purchased from Aladdin Reagent (China) Co., Ltd. Other materials used in the research were of analytical grade. Ultrapure water was used throughout the study.

2.2. Synthesis of $\text{Fe}_3\text{O}_4@\text{SiO}_2@\text{CeO}_2$ catalyst

2.2.1. Synthesis of Fe_3O_4 nanoparticles

Fe_3O_4 magnetic nanoparticles were prepared based on Matijevic's method [41]. Before synthesis, the doubly distilled water was deoxygenated by bubbling N_2 gas for 1 h. In a typical procedure, KNO_3 (10.12 g) and KOH (5.62 g) were dissolved in 400 mL of distilled water, then, 100 mL of 0.2 mol/L FeSO_4 was added dropwise under vigorous stirring in a three-neck flask equipped with constant temperature bath (60 °C) and nitrogen protection. After 4 h stirring, the black precipitate was generated, then, washed with absolute ethanol and distilled water several times and separated by magnetic force. The magnetic nanoparticles were dried under vacuum at 70 °C for 12 h.

2.2.2. Synthesis of $\text{Fe}_3\text{O}_4@\text{SiO}_2$ nanoparticles

Firstly, 1 g of Fe_3O_4 nanoparticles was dispersed in 50 mL of 0.5 mol/L trisodium citrate by ultra-sonication, and then the slurry was continuously stirred with N_2 protection at 60 °C for 6 h. The black precipitate was then washed with absolute ethanol and distilled water several times and separated by magnetic force and was dried under vacuum at 70 °C for 12 h. Secondly, a mixture of

ethanol (80 mL) and distilled water (20 mL) was added to modified Fe_3O_4 (1 g), and then was sonicated for 10 min for Fe_3O_4 dispersion. After adding 5 mL $\text{NH}_3 \cdot \text{H}_2\text{O}$ and 5 mL TEOS, the slurry was under mechanically stirred continuously for 2 h at room temperature. The $\text{Fe}_3\text{O}_4@\text{SiO}_2$ nanoparticles were collected and rinsed with ethanol and distilled water several times, and then dried at 70 °C for 12 h.

2.2.3. Synthesis of $\text{Fe}_3\text{O}_4@\text{SiO}_2@\text{CeO}_2$ nanoparticles

$\text{Fe}_3\text{O}_4@\text{SiO}_2@\text{CeO}_2$ nanoparticles were synthesized via a chemical precipitation and subsequent calcination process. First, approximately 0.232 g of $\text{Fe}_3\text{O}_4@\text{SiO}_2$ nanoparticles was dispersed in 100 mL of 0.05 mol/L cerous nitrate and then the slurry was sonicated for 0.5 h, followed by adding 50 mL of 0.5 mol/L KOH dropwise under continuously stirring in a four-neck flask for 2 h. After vacuum filtration, the precipitate was washed with ethanol and distilled water several times, and then dried at 70 °C for 12 h. Subsequently the dried powder was calcined in a tube furnace from ambient temperature to 500 °C at a heating rate of 5 °C/min and kept at that temperature for 2 h. Nitrogen was used as the protective gas during calcination and the flow rate was 0.2 L/min. After calcination, the $\text{Fe}_3\text{O}_4@\text{SiO}_2@\text{CeO}_2$ nanoparticles were obtained. The schematic illustration of the preparation of $\text{Fe}_3\text{O}_4@\text{SiO}_2@\text{CeO}_2$ magnetic nanoparticles is shown in Fig. 1.

2.3. Characterizations of the magnetic nanoparticles

The morphologies of Fe_3O_4 , $\text{Fe}_3\text{O}_4@\text{SiO}_2$, and $\text{Fe}_3\text{O}_4@\text{SiO}_2@\text{CeO}_2$ nanoparticles were characterized by transmission electronic microscopy (TEM) and scanning electronic microscopy (SEM). The samples for TEM were obtained by placing drops of each sample on a copper grid. Element composition of samples was determined by energy-dispersive X-ray spectrum (EDX). Powder X-ray diffraction (XRD) of the catalyst was recorded on a Thermo ARL SCINTAG X'TRA diffractometer at room temperature using $\text{Cu K}\alpha$ irradiation at 45 kV and 40 mA. Fourier transform-infrared (FT-IR) spectra of the samples was recorded on a Nicolet Magna-IR 6700 spectrometer operating at 32 scans, 2 cm^{-1} resolution in the 4000–450 cm^{-1} wave number region.

2.4. Catalytic ozonation activity measurements

The experimental apparatus employed in this work consisted of a cylindrical Pyrex glass reactor, an O_3 supply system and an exhaust treatment system. The ozone diffuser, fixed at the center of the bottom of the reactor, was a spherical unit with coarse porosity. As ozone diffusing, catalysts could be diffused well in aqueous solution. Experiments were carried out at room temperature. Simulated wastewater containing ASA was added into the reactor. The reaction started with simultaneous $\text{Fe}_3\text{O}_4@\text{SiO}_2@\text{CeO}_2$ catalysts and ozone addition. Samples were withdrawn at predetermined time-points from the top of the reactor, and filtered through a 0.22 μm pore size membrane filter, and then analyze.

The concentrations of ASA were immediately determined by HPLC (Model 1200, Agilent Technologies, USA) equipped with a C18 reversed phase column (Eclipse XDB, Agilent Technologies, USA). The mobile phase was water (mixed with 20% (V%) acetonitrile, 5% (V%) tetrahydrofuran and 5% (V%) acetic acid) and acetonitrile

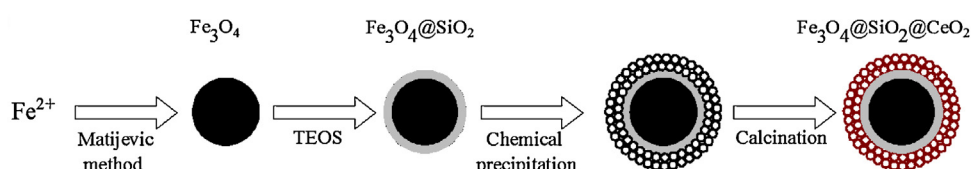


Fig. 1. Synthetic route of $\text{Fe}_3\text{O}_4@\text{SiO}_2@\text{CeO}_2$ magnetic nanoparticles.

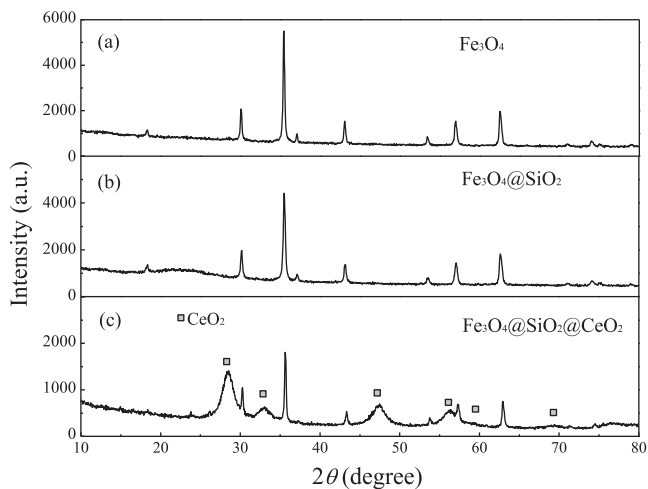


Fig. 2. X-ray diffractograms of (a) pure Fe_3O_4 , (b) $\text{Fe}_3\text{O}_4@\text{SiO}_2$ and (c) $\text{Fe}_3\text{O}_4@\text{SiO}_2@\text{CeO}_2$.

(20:80, v/v). The eluent was delivered at a flow rate of 0.8 mL/min and the absorbance at 276 nm was measured. Total organic carbon (TOC) was analyzed by a TOC-V_{CPH} analyzer. Other intermediates were detected by GC/MS (GC7899/MS5975, Agilent Technologies, USA) with the column of HP-5 (30 m × 0.32 mm × 0.25 μm). The GC column was operated at 50 °C for 2 min and then increased to 300 °C at the rate of 20 °C/min and held at that temperature for 5 min. The other experimental conditions were: EI impact ionization, 70 eV; helium as the carrier gas; injection temperature, 250 °C; source temperature, 220 °C. The concentration of O_3 in liquid phase was determined using an indigo method [42]. The concentration of iron and cerium in solution was determined using a Perkin-Elmer Elan DRC-e ICP-MS instrument.

3. Results and discussion

3.1. XRD and FT-IR analysis of the samples

XRD is an effective method for identifying the phases present in the prepared catalysts [38]. Fig. 2 shows the XRD patterns of the nanoparticles at different steps: (a) Fe_3O_4 nanoparticles, (b) $\text{Fe}_3\text{O}_4@\text{SiO}_2$ nanoparticles and (c) $\text{Fe}_3\text{O}_4@\text{SiO}_2@\text{CeO}_2$ nanoparticles. As shown in Fig. 2a, the XRD results of the iron oxide were just the same as the standard card of Fe_3O_4 (JCPDS No. 72-2303). In other word, the product of first step was magnetite. The characteristic reflections of (a) Fe_3O_4 nanoparticles was assigned to the (1 1 1), (2 2 0), (3 1 1), (2 2 2), (4 0 0), (4 2 2), (5 1 1), (4 4 0) and (5 3 3) planes of the cubic spinel structure with space group $Fd\text{-}3m$ (2 2 7) at 2θ values of approximately 18.3, 30.1, 35.4, 37.0, 43.0, 53.4, 56.9, 62.5, and 73.9, respectively. Compared with Fig. 2a, after being coated by SiO_2 , the intensity of the Fe_3O_4 phase decreased obviously and a wide diffraction of SiO_2 could be found but not significant between 20 and 30 of 2θ values, as shown in Fig. 2b. No sharp diffraction peaks corresponding to SiO_2 can be seen in the pattern reveal that SiO_2 is amorphous [43]. For the $\text{Fe}_3\text{O}_4@\text{SiO}_2@\text{CeO}_2$ sample shown in Fig. 2c, the new diffraction peaks were observed at 2θ values of approximately 28.6, 33.1, 47.6, 56.5, 59.3, and 69.6, corresponding to CeO_2 . In addition, the diffraction peaks of Fe_3O_4 and SiO_2 are also observed in Fig. 2c, but the intensity of the peaks related to the above two figures was further attenuated because of CeO_2 coated.

FT-IR is an appropriate technique to study the chemical adsorption or chemical interaction [44]. Fig. 3 shows the FT-IR spectra of the Fe_3O_4 , $\text{Fe}_3\text{O}_4@\text{SiO}_2$ and $\text{Fe}_3\text{O}_4@\text{SiO}_2@\text{CeO}_2$ particles. In the case of Fe_3O_4 (curve a), the broad bands centered around 3428

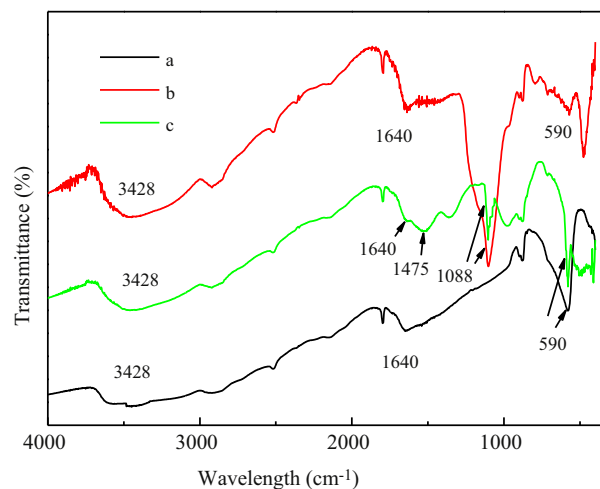


Fig. 3. FT-IR spectra of (a) Fe_3O_4 , (b) $\text{Fe}_3\text{O}_4@\text{SiO}_2$ and (c) $\text{Fe}_3\text{O}_4@\text{SiO}_2@\text{CeO}_2$ particles.

and 1640 cm⁻¹ are assigned to the H—O—H stretching modes and bending vibration of the free or adsorbed water, respectively [39]. And the characteristic absorption peak at 590 cm⁻¹ is attributed to the Fe—O structure. In the case of $\text{Fe}_3\text{O}_4@\text{SiO}_2$ nanoparticles (curve b) the sharp band at 1088 cm⁻¹ is corresponding to Si—O—Si antisymmetric stretching vibrations, being indicative of the existence of SiO_2 in the $\text{Fe}_3\text{O}_4@\text{SiO}_2$ nanoparticles [45]. In the case of $\text{Fe}_3\text{O}_4@\text{SiO}_2@\text{CeO}_2$ nanoparticles (curve c) the band around 1475 cm⁻¹ is corresponding to Ce—O vibrations, indicating of the existence of CeO_2 in the $\text{Fe}_3\text{O}_4@\text{SiO}_2@\text{CeO}_2$ nanoparticles. In addition, the O—H stretching band at 3428 and 1640 cm⁻¹ are still existed in the spectrum of $\text{Fe}_3\text{O}_4@\text{SiO}_2$ (curve b) and $\text{Fe}_3\text{O}_4@\text{SiO}_2@\text{CeO}_2$ (curve c), which may be related to the free or adsorbed water. Moreover, the characteristic absorption peak at 590 and 1088 cm⁻¹ can also be observed in curve c, but the transmittance was relatively diminished because of CeO_2 coated.

3.2. TEM, SEM and EDX studies of the samples

TEM and SEM were similar analytical techniques used for understanding the morphologies and structures of the products at different synthetic steps [46]. Fig. 4a–c shows the TEM images of Fe_3O_4 , $\text{Fe}_3\text{O}_4@\text{SiO}_2$ and $\text{Fe}_3\text{O}_4@\text{SiO}_2@\text{CeO}_2$, respectively. As shown in Fig. 4a, it shows a representative TEM image of Fe_3O_4 nanoparticles, clearly indicating that the nanoparticles display an irregular shape with an average diameter of about 150 nm. The inset high resolution image (Fig. 4a) of the nanoparticles demonstrates that they are well-crystallized. Seen from the TEM image of $\text{Fe}_3\text{O}_4@\text{SiO}_2$ particles (Fig. 4b), the core–shell structure could be clearly observed and the thickness of the SiO_2 layer is about 50 nm. The inset HRTEM image (Fig. 4b) of the nanoparticles illustrates that the surfaces of the microspheres are smooth, and the nanoparticles change into a spherical shape, wrapped with a nonporous coherent layer of the homogeneous silica. The layer of the homogeneous silica can avoid the inner magnetic iron oxide core to be oxidized [38,40]. As shown in Fig. 4c, many $\text{Fe}_3\text{O}_4@\text{SiO}_2$ particles are successfully encapsulated in the ceria layer, obtained $\text{Fe}_3\text{O}_4@\text{SiO}_2@\text{CeO}_2$ nanoparticles. As a result of the aggregation of partial $\text{Fe}_3\text{O}_4@\text{SiO}_2@\text{CeO}_2$, the diameters of particles range from 230 to 250 nm and the thickness of the CeO_2 layer is about 30–50 nm. The inset HRTEM image (Fig. 4c) of the nanoparticles shows a relatively rough but still coherent coating ceria layer, which is located in the edges of the particles, and the $\text{Fe}_3\text{O}_4@\text{SiO}_2$ particle is still seen in the middle.

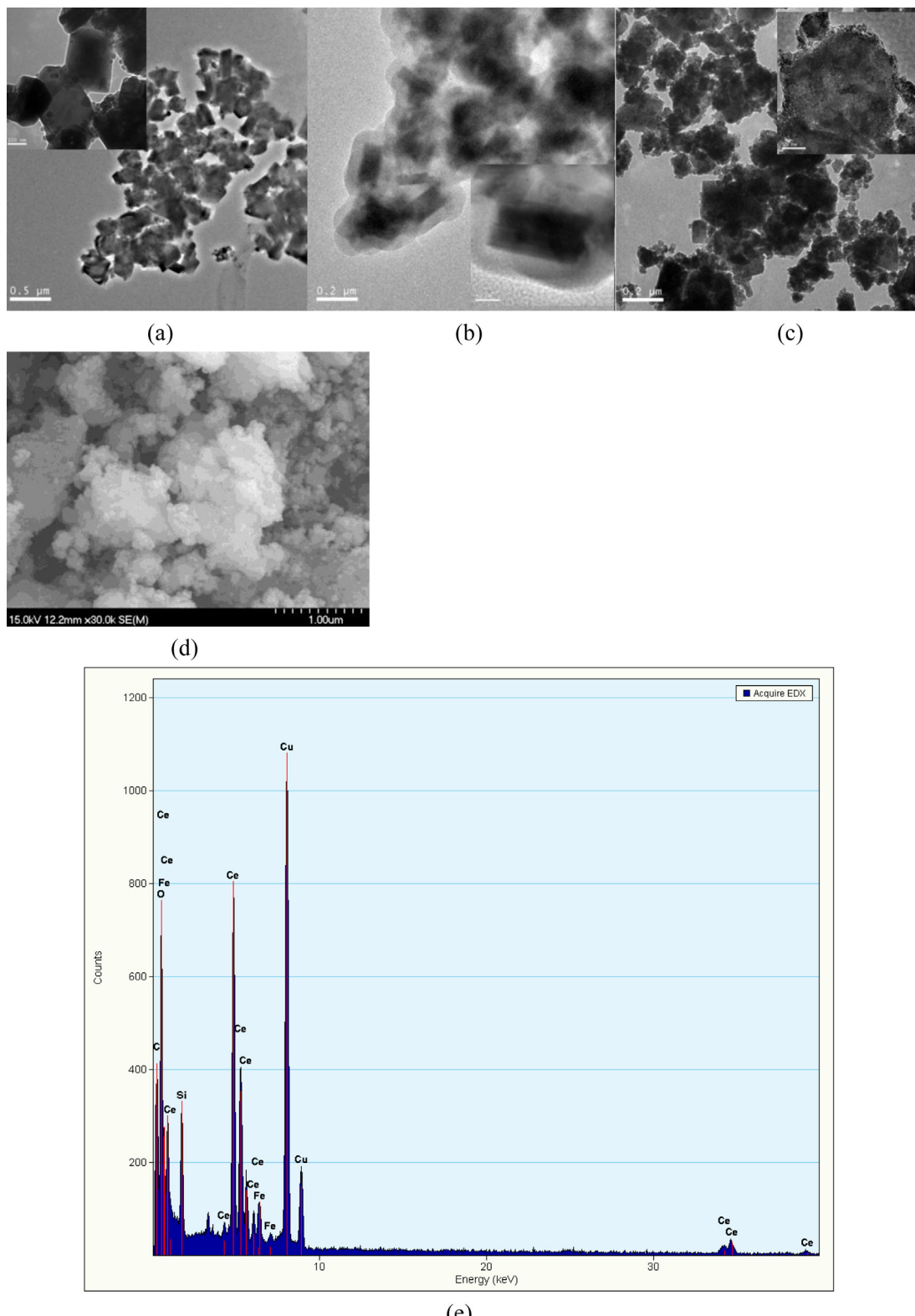


Fig. 4. TEM images of (a) Fe₃O₄ microspheres, (b) Fe₃O₄@SiO₂ microspheres and (c) Fe₃O₄@SiO₂@CeO₂ microspheres; SEM image of (d) Fe₃O₄@SiO₂@CeO₂ microspheres; EDX spectrum image of (e) Fe₃O₄@SiO₂@CeO₂ microspheres.

Typical SEM image (Fig. 4d) of the Fe₃O₄@SiO₂@CeO₂ show that the as-fabricated samples mainly exhibit aggregates of different shapes, each formed by smaller particles having quite spherical shape, demonstrating that CeO₂ nanoparticles which have the property of catalytic ozonation are successfully assembled on the

surfaces of the magnetic cores. EDX was used for the elemental analysis or chemical characterization of a sample [30]. The CeO₂ shell can be further confirmed from the EDX (Fig. 4e) since the Fe₃O₄@SiO₂@CeO₂ nanoparticles are seen to be composed of Fe, O, Si and Ce (Cu arising from the copper grid and C from the adhesive).

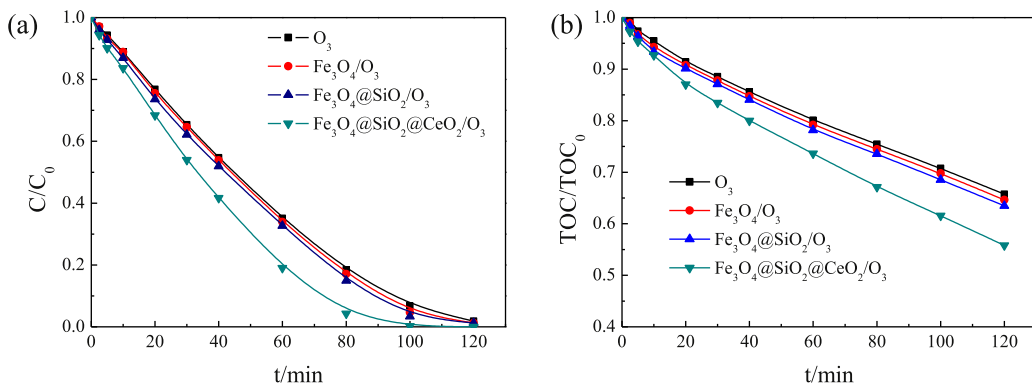


Fig. 5. Catalytic performance of various samples of catalysts: (a) the efficiency of ASA removal; (b) the efficiency of TOC removal.

3.3. The catalytic activity measurements for ozonation of ASA

To evaluate the catalytic activity of various samples of catalysts, the catalytic degradation of ASA in the presence of catalyst was carried out. Fig. 5a shows the efficiency of ASA removal over the course of the reaction using various samples. The results showed that after 60 min, the ASA removal with Fe₃O₄@SiO₂@CeO₂ catalyst could reach 81.0%, while 67.3% with Fe₃O₄@SiO₂ catalyst, 66.1% with Fe₃O₄ catalyst and only 64.1% with ozonation alone, indicating that Fe₃O₄@SiO₂@CeO₂ is an effective catalyst for catalytic ozonation of ASA.

Fig. 5b shows the efficiency of TOC removal using various samples. As shown in Fig. 5b, within the 120 min period, TOC was removed only by 36.5% in the presence of Fe₃O₄@SiO₂ and only by 35.4% in the presence of Fe₃O₄, which was close to that of the ozonation without catalyst (34.2%). However, when adding Fe₃O₄@SiO₂@CeO₂ catalyst, the TOC removal was greatly enhanced and reached 44.2%. The kinetic analysis showed that the results of TOC removal were followed the pseudo-first order reaction. The reaction constants varied from $3.2 \times 10^{-3} \text{ min}^{-1}$ of the ozonation without catalyst to $4.8 \times 10^{-3} \text{ min}^{-1}$ of the ozonation with Fe₃O₄@SiO₂@CeO₂ in 120 min. And after 240 min, TOC removal reached 43.4% in the presence of Fe₃O₄@SiO₂, 41.9% in the presence of Fe₃O₄ and 39.4% of only ozonation without catalyst. While when adding Fe₃O₄@SiO₂@CeO₂ catalyst, the TOC removal was significantly upgraded and reached 67.2% after 240 min. The longer the reaction time is, the more significant difference between the efficiency of catalytic ozonation by Fe₃O₄@SiO₂@CeO₂ and the efficiency of ozonation alone will be. Overall, the results demonstrate that Fe₃O₄@SiO₂@CeO₂ can not only enhance the ASA removal but also enhance the mineralization, and a high mineralization is achieved using CeO₂ based catalyst.

3.4. Ozone consumption

The mass balance of ozone in gas and liquid phase can be described using the following expression [47]:

$$[O_3]_T = [O_3]_0 + [O_3]_R + [O_3]_C \quad (1)$$

where [O₃]_T is the concentration of total applied ozone; [O₃]₀ is the concentration of off gas ozone; [O₃]_R is the concentration of residual ozone and [O₃]_C is the concentration of consumed ozone.

As a matter of convenience to evaluate, the dimension of Eq. (1) is transferred from mg to mg/L uniformly. At first 10 min, 20 min and 30 min, we tested that [O₃]_T, [O₃]₀ and [O₃]_R in O₃ alone, Fe₃O₄/O₃, Fe₃O₄@SiO₂/O₃ and Fe₃O₄@SiO₂@CeO₂/O₃ processes were listed in Table 1.

Based on the data in Table 1, [O₃]_C can be calculated from Eq. (1). Therefore, R_U, the utilization efficiency of ozone, can be expressed as follows:

$$R_U = \frac{[O_3]_C}{[O_3]_T} \quad (2)$$

According to the results obtained and Eq. (2), the evolution of R_U with amount of Fe₃O₄@SiO₂@CeO₂ catalyst corresponding to the experiment studied is 54.1%, 46.8%, 36.3% and 36.8%, 27.1%, 18.8% with ozonation alone at first 10 min, 20 min, and 30 min, respectively. The ozone utilization with Fe₃O₄@SiO₂@CeO₂ catalyst is more efficiency than that with ozonation alone. From Table 1 it also can be observed that, with the same amount of catalyst, ozone/Fe₃O₄@SiO₂@CeO₂ can obtain a higher R_U compared to the case of ozone/Fe₃O₄ and ozone/Fe₃O₄@SiO₂. With all of ASA and other phenyl intermediates removed and transformed to saturated carboxylic acids, the utilization efficiency of ozone become lower, but R_U with Fe₃O₄@SiO₂@CeO₂ catalyst is still more efficiency than that with ozonation alone, ozone/Fe₃O₄ and ozone/Fe₃O₄@SiO₂. According to this phenomenon, it can be deduced that Fe₃O₄@SiO₂@CeO₂ has the higher catalytic activity to improve R_U in the ozonation system. The results, the decrease in [O₃]₀, almost the same in [O₃]_R and the increase in R_U in each time, may suggest that both ozone and organic molecules adsorb by the catalyst and then undergoes a surface reaction.

Generally, there are two possible reaction mechanisms of catalysts for the heterogeneous catalytic ozonation of organic compounds: (1) Catalysts could increase the HO[•] generation, which then reacts with organic compounds to form oxidized products or intermediate products; (2) The other way is that both ozone and organic molecules adsorb by the catalyst and then undergoes a surface reaction [15,48–50].

In order to verify whether the ozonation of ASA in the presence of Fe₃O₄@SiO₂@CeO₂ catalyst involves HO[•] radicals, some experiments were also carried out in the presence of 10 mmol/L TBA (*tert*-butyl alcohol), because TBA is a radical scavenger and it can react with HO[•] rapidly. Fig. 6 shows that, after adding TBA, the degradation rate of ASA did not significantly change. So we believe that the high removal efficiency of ASA was attributed to surface reaction. And due to the coating layer of ceria, the adsorption equilibrium of ozone and organics in the coating layer can be shifted toward higher concentration and therefore the oxidation reaction is boosted in the surface of catalyst, comparing with regular aquatic reactions [23–27].

3.5. Probable degradation pathway

A lot of intermediates were generated during the catalytic ozonation process. Intermediates were detected by GC/MS, IC and

Table 1

The values of $[O_3]_0$, $[O_3]_R$ and R_U in catalytic ozonation by different catalysts.

Catalytic ozonation by different catalysts	10 min			20 min			30 min		
	$[O_3]_0$	$[O_3]_R$	R_U (%)	$[O_3]_0$	$[O_3]_R$	R_U (%)	$[O_3]_0$	$[O_3]_R$	R_U (%)
Ozonation alone	28.4	1.9	36.8	32.6	2.4	27.1	36.2	2.8	18.8
Fe_3O_4	28.3	1.8	37.1	31.9	2.4	28.5	35.6	2.7	20.1
$Fe_3O_4@SiO_2$	26.4	1.8	41.3	31.2	2.3	30.2	35.0	2.7	21.4
$Fe_3O_4@SiO_2@CeO_2$	20.5	1.5	54.1	23.5	2.0	46.8	28.2	2.4	36.3

The units of $[O_3]_0$ and $[O_3]_R$ are mg/L. $[O_3]_R$ is 48 mg/L.

Table 2

Intermediate compounds.

Symbol	Compounds	Structural formula	Analysis methods
D ₁	Acetylsalicylic acid		HPLC, GC/MS
D ₂	Salicylic acid		GC/MS
D ₃	Phenol		GC/MS
D ₄	p-Dihydroxybenzene		GC/MS
D ₅	o-Dihydroxybenzene		GC/MS
D ₆	Maleic acid		HPLC, GC/MS
D ₇ D ₈ D ₉	Fumaric acid Succinic acid Acetic acid		HPLC, GC/MS HPLC, GC/MS IC

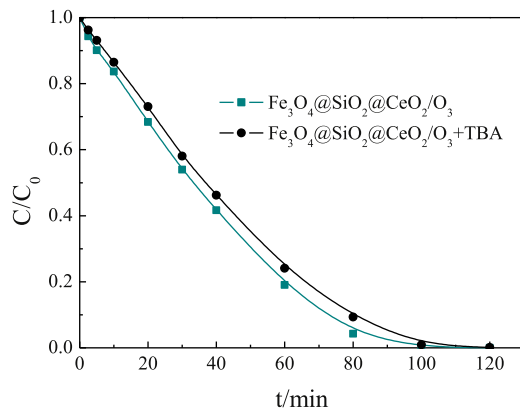


Fig. 6. The effect of added TBA on catalytic ozonation of ASA.

HPLC, Table 2 shows the intermediates detected in this experiment. On the basis of the intermediates formed in the process of degradation, a probable pathway is proposed and is outlined in Fig. 7.

In heterogeneous system, the surface reaction plays the key role during ASA degradation in ozonation. In the degradation, the attack of catalyst or O_3 on the C–O bond of ASA yielded salicylic acid (D₂) and acetic acid, and then D₂ transformed to phenol (D₃) because of decarboxylation. D₃ could be further attacked by catalyst or O_3 on the benzene of ortho-position and para-position, forming o-dihydroxybenzene (D₄) and p-dihydroxybenzene (D₅). Due to self-electron transfer in the molecule, D₄ and D₅ were transferred to S₁ and S₂. By benzene ring cleaving, they were decomposed to succinic, maleic and fumaric acids, which could be further decomposed to acetic and oxalic acids. These acids were gradually decomposed to formic acid. Finally, the formic acid was decomposed to CO_2 and H_2O .

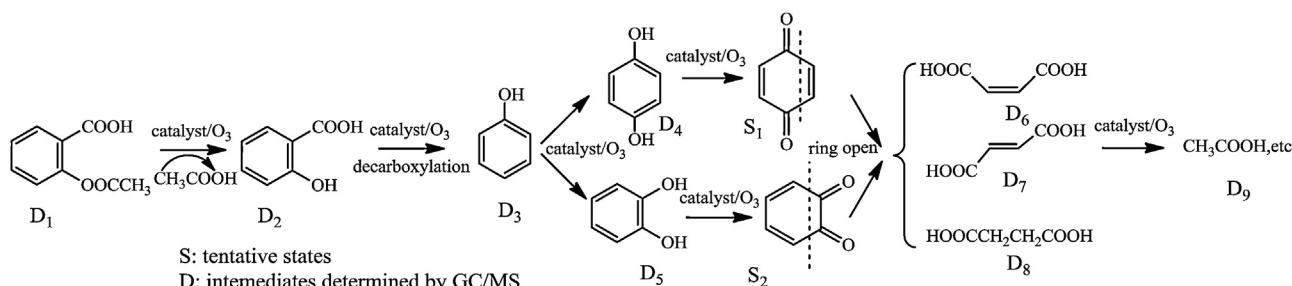


Fig. 7. The probable degradation pathway of ASA by catalytic ozonation.

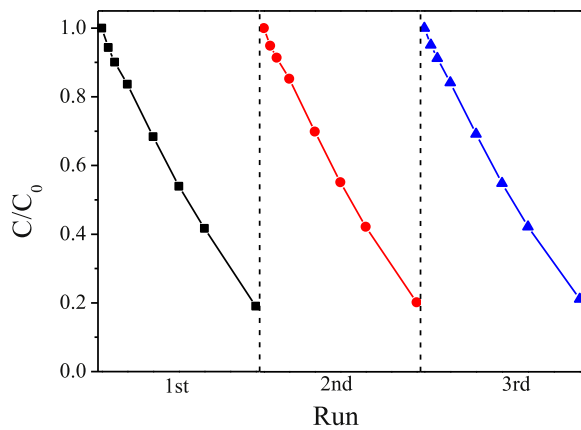


Fig. 8. Ozonation of ASA for 3 successive reactions catalyzed with the same batch of $\text{Fe}_3\text{O}_4@\text{SiO}_2@\text{CeO}_2$ catalyst.

3.6. Catalyst stability

Considering real applications in the future, stability and recyclability of the $\text{Fe}_3\text{O}_4@\text{SiO}_2@\text{CeO}_2$ catalysts deserve careful attention and have been investigated. Therefore, three continuous cycles for catalytic ozonation of acetylsalicylic acid using $\text{Fe}_3\text{O}_4@\text{SiO}_2@\text{CeO}_2$ catalysts under identical conditions were carried out. After finishing one cycle, a combination of magnetic separation and centrifugation enable the catalysts to be collected from the mixture to catalyze a new cycle. Fig. 8 shows ozonation of ASA for 3 successive reactions catalyzed with the same batch of $\text{Fe}_3\text{O}_4@\text{SiO}_2@\text{CeO}_2$ catalyst. As shown in Fig. 8, the catalytic activity of $\text{Fe}_3\text{O}_4@\text{SiO}_2@\text{CeO}_2$ did not significantly decrease in the three continuous cycles, in which the degradation of ASA was found to be 81.0%, 79.8% and 78.9%, respectively, after 60 min, revealing the high activity and stability of the magnetic nanocatalysts.

Leaching of cerium and iron from $\text{Fe}_3\text{O}_4@\text{SiO}_2@\text{CeO}_2$ catalyst during catalytic ozonation of acetylsalicylic acid is another stability test of catalyst [51]. From ICP-MS test results, at a reaction time of 120 min, the concentrations of cerium and iron in aqueous solution are 0.13 and 0.35 mg/L, respectively. It can be deduced that cerium and iron are stable on the catalyst at the reaction conditions as the metal leached are rather low.

4. Conclusions

The $\text{Fe}_3\text{O}_4@\text{SiO}_2@\text{CeO}_2$ catalysts with the structure of a Fe_3O_4 magnetic core, a silica membrane mid-layer and CeO_2 outer layer were prepared in this study, and the structure of $\text{Fe}_3\text{O}_4@\text{SiO}_2@\text{CeO}_2$ catalysts were confirmed by XRD, FT-IR, TEM, SEM and EDX. Magnetic $\text{Fe}_3\text{O}_4@\text{SiO}_2@\text{CeO}_2$ catalysts which can be separated easily by magnetic force were used for catalytic ozonation for the degradation of ASA in aqueous solution. $\text{Fe}_3\text{O}_4@\text{SiO}_2@\text{CeO}_2$ catalysts were more efficient catalytic ozonation activity than ozone alone in the degradation of ASA and could also enhance the TOC removal efficiency. The ASA removal with $\text{Fe}_3\text{O}_4@\text{SiO}_2@\text{CeO}_2$ catalyst at 60 min could reach 81.0%, while 67.3% with $\text{Fe}_3\text{O}_4@\text{SiO}_2$ catalyst, 66.1% with Fe_3O_4 catalyst and only 64.1% with ozonation alone. The reaction mechanism of catalytic ozonation over $\text{Fe}_3\text{O}_4@\text{SiO}_2@\text{CeO}_2$ develops mainly through surface reactions and this may be indicative of the absence of an aqueous hydroxyl radical pathway in catalytic ozonation over a $\text{Fe}_3\text{O}_4@\text{SiO}_2@\text{CeO}_2$ catalyst, which was confirmed by the fact that the presence of radical scavengers did not affect the degradation efficiency. Intermediates such as salicylic acid, phenol, *p*-dihydroxybenzene, *o*-dihydroxybenzene, succinic acid, maleic acid, fumaric acid and acetic acid were detected by GC/MS and a possible degradation pathway was suggested.

Moreover, the $\text{Fe}_3\text{O}_4@\text{SiO}_2@\text{CeO}_2$ catalysts had magnetic recyclability and low metal leaching. Overall, these advantages make the $\text{Fe}_3\text{O}_4@\text{SiO}_2@\text{CeO}_2$ catalysts promising applications in catalytic ozonation of wastewater.

Acknowledgements

The authors are grateful for the financial support provided by the National Natural Science Foundation of China (21306175), the Project of Science and Technology Office of Zhejiang Province (No. 2008C13014-6), Natural Science Foundation of Zhejiang Province (LY13E080017), and the Research Fund for the Doctoral Program of Higher Education of China (No. 20113317120004).

References

- [1] M.M. Huber, S. Canonica, G.Y. Park, U.V. Gunten, Environmental Science and Technology 37 (2003) 1016–1024.
- [2] T.A. Ternes, J. Stuber, N. Herrmann, D. McDowell, A. Ried, M. Kampmann, B. Teiser, Water Research 37 (2003) 1976–1982.
- [3] S. Esplugas, D.M. Bila, L.G.T. Krause, M. Dezotti, Journal of Hazardous Materials 149 (2007) 631–642.
- [4] J.N. Wu, T.W. Wang, Water Research 35 (2001) 1093–1099.
- [5] R. Andreozzi, M. Canterino, R. Marotta, N. Paxeus, Journal of Hazardous Materials 122 (2005) 243–250.
- [6] J. Rivera-Utrilla, M. Sanchez-Polo, Applied Catalysis B: Environmental 39 (2002) 319–329.
- [7] B. Kasprzyk-Hordern, M. Ziolek, J. Nawrocki, Applied Catalysis B: Environmental 46 (2003) 639–669.
- [8] R. Thiruvenkatachari, T.O. Kwon, J.C. Jun, S. Balaji, M. Matheswaran, I.S. Moon, Journal of Hazardous Materials 142 (2007) 308–314.
- [9] B. Legube, N.K.V. Leitner, Catalysis Today 53 (1999) 61–72.
- [10] S. Song, M. Xia, Z.Q. He, H.P. Ying, B.S. Lu, J.M. Chen, Journal of Hazardous Materials 144 (2007) 532–537.
- [11] A. Latifoglu, M.D. Gurol, Water Research 37 (2003) 1879–1889.
- [12] E.J. Rosenfeldt, K.G. Linden, S. Canonica, U.V. Gunten, Water Research 40 (2006) 3695–3704.
- [13] Z.Q. He, A.L. Zhang, S. Song, Z.W. Liu, J.M. Chen, X.H. Xu, W.P. Liu, Industrial and Engineering Chemistry Research 49 (2010) 12345–12351.
- [14] C. Hu, S.T. Xing, J.H. Qu, H. He, Journal of Physical Chemistry C 112 (2008) 5978–5983.
- [15] F.J. Beltran, F.J. Rivas, R. Montero-de-Espinosa, Industrial and Engineering Chemistry Research 42 (2003) 3218–3224.
- [16] F.J. Beltran, F.J. Rivas, R. Montero-de-Espinosa, Journal of Chemical Technology and Biotechnology 78 (2003) 1225–1233.
- [17] P.C.C. Faria, D.C.M. Monteiro, J.J.M. Orfao, M.F.R. Pereira, Chemosphere 74 (2009) 818–824.
- [18] F.J. Beltran, F.J. Rivas, R. Montero-de-Espinosa, Applied Catalysis B: Environmental 47 (2004) 101–109.
- [19] S.M. Avramescu, C. Bradu, I. Udrea, N. Mihalache, F. Ruta, Catalysis Communications 9 (2008) 2386–2391.
- [20] J.H. Qu, H.Y. Li, H.J. Liu, H. He, Catalysis Today 90 (2004) 291–296.
- [21] X. Zhai, Z.L. Chen, S.Q. Zhao, H. Wang, L. Yang, Journal of Environmental Sciences 22 (2010) 1527–1533.
- [22] E.C. Chetty, V.B. Dasireddy, S. Maddila, S.B. Jonnalagadda, Applied Catalysis B: Environmental 117–118 (2012) 18–28.
- [23] P.C.C. Faria, J.J.M. Orfao, M.F.R. Pereira, Catalysis Communications 9 (2008) 2121–2126.
- [24] L.S. Li, W.Y. Ye, Q.Y. Zhang, F.Q. Sun, P. Lu, X.K. Li, Journal of Hazardous Materials 170 (2009) 411–416.
- [25] R.C. Martins, R.M. Quinta-Ferreira, Applied Catalysis B: Environmental 90 (2009) 268–277.
- [26] R.C. Martins, R.M. Quinta-Ferreira, Industrial and Engineering Chemistry Research 48 (2009) 1196–1202.
- [27] C.A. Orge, J.J.M. Orfao, M.F.R. Pereira, A.M.D. Farias, M.A. Fraga, Chemical Engineering Journal 200–202 (2012) 499–505.
- [28] T.T. Baby, S. Ramaprabhu, Talanta 80 (2010) 2016–2022.
- [29] S.H. Xuan, F. Wang, X.L. Gong, S.K. Kong, J.C. Yu, K.C. Leung, Chemical Communications 47 (2011) 2514–2516.
- [30] G. Cheng, J.L. Zhang, Y.L. Liu, D.H. Sun, J.Z. Ni, Chemical Communications 47 (2011) 5732–5734.
- [31] A.H. Lv, C. Hu, Y.L. Nie, J.H. Qu, Applied Catalysis B: Environmental 100 (2010) 62–67.
- [32] M.L. Luo, D. Bowden, P. Brimblecombe, Applied Catalysis B: Environmental 87 (2009) 1–8.
- [33] Y.M. Ren, Q. Dong, J. Feng, J. Ma, Q. Wen, M.L. Zhang, Journal of Colloid and Interface Science 382 (2012) 90–96.
- [34] S.H. Sun, H. Zeng, D.B. Robinson, S. Raoux, P.M. Rice, S.X. Wang, G.X. Li, Journal of the American Chemical Society 126 (2004) 273–279.

- [35] Z.D. Zhang, J.G. Zheng, I. Skorvanek, G.H. Wen, J. Kovac, F.W. Wang, J.L. Yu, Z.J. Li, X.L. Dong, S.R. Jin, W. Liu, X.X. Zhang, *Journal of Physics: Condensed Matter* 13 (2001) 1921–1929.
- [36] A.L. Morel, S.I. Nikitenko, K. Gionnet, A. Wattiaux, J. Lai-Kee-Him, C. Labrugere, B. Chevalier, G. Deleris, C. Petibois, A. Brisson, M. Simonoff, *ACS Nano* 2 (2008) 847–856.
- [37] L. Zhou, C. Gao, W.J. Xu, *Langmuir* 26 (2010) 11217–11225.
- [38] Z.Q. He, T.M. Hong, J.M. Chen, S. Song, *Separation and Purification Technology* 96 (2012) 50–57.
- [39] G.H. Du, Z.L. Liu, X. Xia, Q. Chu, S.M. Zhang, *Journal of Sol-Gel Science and Technology* 39 (2006) 285–291.
- [40] C.Q. Yang, G. Wang, Z.Y. Lu, J. Sun, J.Q. Zhuang, W.S. Yang, *Journal of Materials Chemistry* 15 (2005) 4252–4257.
- [41] T. Sugimoto, E. Matijevic, *Journal of Colloid and Interface Science* 74 (1980) 227–243.
- [42] H. Bader, J. Hoigne, *Water Research* 15 (1981) 449–456.
- [43] Z.H. Wang, S.Y. Zhu, S.P. Zhao, H.B. Hu, *Journal of Alloys and Compounds* 509 (2011) 6893–6898.
- [44] L.Y. Wang, Y. Sun, J. Wang, J.A. Wang, A.M. Yu, H.Q. Zhang, D.Q. Song, *Colloids and Surfaces B* 84 (2011) 484–490.
- [45] Q. Chang, L.H. Zhu, C. Yu, H.Q. Tang, *Journal of Luminescence* 128 (2008) 1890–1895.
- [46] Y.H. Deng, D.W. Qi, C.H. Deng, X.M. Zhang, D.Y. Zhao, *Journal of the American Chemical Society* 130 (2008) 28–29.
- [47] L. Zhao, J. Ma, Z.Z. Sun, H.L. Liu, *Applied Catalysis B: Environmental* 89 (2009) 326–334.
- [48] F.J. Beltran, F.J. Rivas, L.A. Fernandez, P.M. Alvarez, R.M. Espinosa, *Industrial and Engineering Chemistry Research* 41 (2002) 6510–6517.
- [49] L. Gu, X.W. Zhang, L.C. Lei, *Industrial and Engineering Chemistry Research* 47 (2008) 6809–6815.
- [50] M. Ernst, F. Lurot, J.C. Schrotter, *Applied Catalysis B: Environmental* 47 (2004) 15–25.
- [51] P.M. Alvarez, F.J. Beltran, J.P. Pocostales, F.J. Masa, *Applied Catalysis B: Environmental* 72 (2007) 322–330.